Nanoscale

PAPER

View Article Online
View Journal | View Issue

Cite this: *Nanoscale*, 2020, **12**, 13113

Size- and temperature-dependent photoluminescence spectra of strongly confined $CsPbBr_3$ quantum dots†

Oscar Hsu-Cheng Cheng,[a] Tian Qiao,[a] Matthew Sheldon *[a,b] and Dong Hee Son *[a,c]

Received 6th April 2020,
Accepted 8th June 2020

DOI: 10.1039/d0nr02711a

rsc.li/nanoscale

Lead-halide perovskite nanocrystals (NCs) are receiving much attention as a potential high-quality source of photons due to their superior luminescence properties in comparison to other semiconductor NCs. To date, research has focused mostly on NCs with little or no quantum confinement. Here, we measured the size- and temperature-dependent photoluminescence (PL) from strongly confined $CsPbBr_3$ quantum dots (QDs) with highly uniform size distributions, and examined the factors determining the evolution of the energy and linewidth of the PL with varying temperature and QD size. Compared to the extensively studied II–VI QDs, the spectral position of PL from $CsPbBr_3$ QDs shows an opposite dependence on temperature, with weaker dependence overall. On the other hand, the PL linewidth is much more sensitive to the temperature and size of the QDs compared to II–VI QDs, indicating much stronger coupling of excitons to the vibrational degrees of freedom both in the lattice and at the surface of the QDs.

Introduction

Lead halide perovskites (LHP) nanocrystals (NCs) have emerged as a strong contender for next-generation solid-state emitters[1–5] because of their high luminescence quantum yield,[6–10] facile chemical bandgap tunability,[11,12] and low-cost solution processability.[13,14] Over the past few years, LHP-based light-emitting diodes (LEDs) have reached external quantum efficiencies >20%, which is comparable to organic light-emitting diodes (OLEDs) and other colloidal semiconductor NCs used in commercialized displays.[15,16] For photonic applications of semiconductor NCs, the spectral characteristics of the luminescence, *i.e.* energy and linewidth, is of great importance. Narrow emission bandwidth ensuring high colour purity is desirable for display devices.[17,18] On the other hand, broad or (and) multiple emission peaks covering a wider spectrum is more useful for lighting applications requiring white light.[19,20]

So far, the majority of studies of the luminescence of LHP NCs and related optical properties have been focused on large NCs with weak or no quantum confinement. Therefore, the optical spectra of the NCs exhibit little size dependence. Tuning of the exciton luminescence spectrum was achieved mostly *via* chemical modification of the band, specifically by varying the halide composition and stoichiometry.[21,22] Facile chemical exchange of halides (Cl, Br, and I) enables continuous tuning of the bandgap across the visible spectrum, and thus has been extensively explored as the means of controlling the luminescence colour from LHP NCs. However, phase segregation or migration of halides under photoexcitation have been identified as potential issues for mixed-halide LHP NCs as the source of photons in technological applications.[23–27] More recently, synthetic methods for producing highly uniform LHP nanocrystals with strong quantum confinement were developed.[28–32] Such quantum confinement can be used to vary the exciton transition energy as well as enhance the coupling of excitons to other degrees of freedom, further tuning optical and electronic properties similar to the extensively studied II–VI and IV–VI QDs.[33–36]

Either chemical tuning of the bandgap or size-dependent quantum confinement can vary the colour of the emission from LHP NCs. However, these separate strategies do not have the same effect on all of the characteristics of the exciton luminescence. For instance, reducing the size of strongly confined NCs introduces size-dependent electron–hole interactions and vibronic coupling involving both lattice phonons

[a]*Department of Chemistry, Texas A&M University, College Station, TX 77843, USA. E-mail: dhson@chem.tamu.edu, sheldonm@tamu.edu*
[b]*Department of Material Science & Engineering, Texas A&M University, College Station, TX 77843, USA*
[c]*Center for Nanomedicine, Institute for Basic Science, Graduate Program of Nano Biomedical Engineering, Advanced Science Institute, Yonsei University, Seoul 03722, Republic of Korea*

†Electronic supplementary information (ESI) available. See DOI: 10.1039/d0nr02711a

and surface ligand.[37–39] Therefore, the energy and linewidth of exciton photoluminescence (PL) as well as the temperature dependence and exciton radiative lifetime can be quite different in comparison with non-confined mixed-halide LHP NCs exhibiting the same PL wavelength. Furthermore, the degree of ensemble size uniformity and the larger surface-to-volume ratio in strongly confined QDs can alter the characteristics of the exciton luminescence significantly.[37] Therefore, it is important to understand the spectral characteristics of LHP QDs in the strongly confined regime to understand their potential utility as a source of photons.

Here, we measured the size- and temperature-dependent PL spectra of uniform ensembles of strongly confined $CsPbBr_3$ QDs and investigated the factors that dictate their spectral evolution when varying size and temperature. From the analysis of the temperature dependence of the PL spectral linewidth,[40–43] we obtained information about the effective strength of the coupling of excitons with the vibrational degrees of freedom as a function of the QD size. We also compared our results with those of CdSe QDs, an archetypal QD system with well-known size- and temperature-dependent PL, in order to highlight the unique aspects of the PL from strongly confined $CsPbBr_3$ QDs.

Experimental

Sample preparation

Size-controlled $CsPbBr_3$ QDs were synthesized *via* the hot-injection method reported in ref. 28. The synthesized QDs were purified using ethyl acetate to remove all remaining unreacted precursors and excess ligands by centrifuging the solution at 3500 rpm at 5 min. The precipitate was recovered and redispersed in hexane for all spectroscopic measurements in solution sample and preparation of QD film on a sapphire substrate.

Temperature dependent PL measurement

Temperature-dependent PL measurements were made using an open-cycle cryostat (ST-100, Janis) using liquid nitrogen and liquid helium as the cryogen. The QD film on sapphire substrate was excited at 405 nm using a cw diode laser (RGBLase, FBB-405-200-FM-E-1-0). The excitation power was kept below ~1 mW with a 3 mm beam diameter to avoid heating of the substrate. The PL spectra were recorded with two different CCD spectrometers (QE65000, Ocean Optics and WiTec alpha 300), which give identical line shape after the calibration of the spectral response of each spectrometer. A 405 nm notch filter was used to block the excitation light in PL spectrum measurement and its transmission spectrum was accounted for in the analysis of the PL spectra.

Results and discussion

In this study, highly uniform ensembles of $CsPbBr_3$ QDs were prepared using the recently developed method that leverages thermodynamic equilibrium for the precise size control in strongly confined regime, which minimizes the effect of size dispersity on the PL spectra.[28] $CsPbBr_3$ QDs of varying sizes prepared in this study exhibit well-resolved confined exciton absorption and emission spectra as shown in Fig. 1(a). The edge length (d) of the QDs determined by transmission electron microscopy (TEM) images (Fig. 1(b)–(e)) are in the range of 3.9 to 6.3 nm, which is smaller than twice the exciton Bohr radius of $CsPbBr_3$ ($2a_B$ = 7 nm).[44] For temperature-dependent PL measurements, the $CsPbBr_3$ QDs were deposited on a sapphire substrate by dipping the substrate into concentrated $CsPbBr_3$ QD solutions dispersed in hexane, and then drying with nitrogen gas. The QD film prepared by this method is relatively close-packed with interparticle spacing of ~3 nm corresponding to the organic ligand on the surface of the QDs. Fig. 2 compares the PL spectra of the colloidal solution of $CsPbBr_3$ QDs in hexane and the QD film deposited on a sapphire substrate. The PL spectra of $CsPbBr_3$ QDs in these different environments are nearly identical, while the film of the smallest QDs (d = 3.9 nm) exhibit a small blueshift compared to the solution of QDs. The similarity of the spectra from NCs in solution and deposited as films indicates a lack of interparticle electronic coupling. Other studies of $CsPbBr_3$

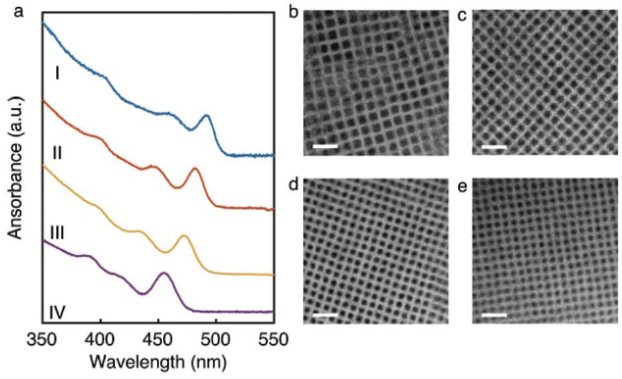

Fig. 1 (a) Absorption spectra of different sizes of $CsPbBr_3$ QDs. (b–d) TEM images of $CsPbBr_3$ QDs. The average edge length of the QDs is (I) 6.3 nm, (II) 5.3 nm, (III) 4.7 nm, (IV) 3.9 nm. All scale bars are 20 nm.

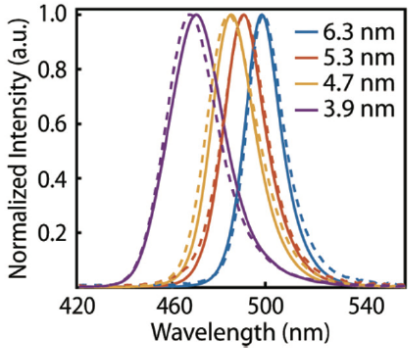

Fig. 2 PL spectra of $CsPbBr_3$ QDs in hexane (solid line) and on sapphire substrate (dash line).

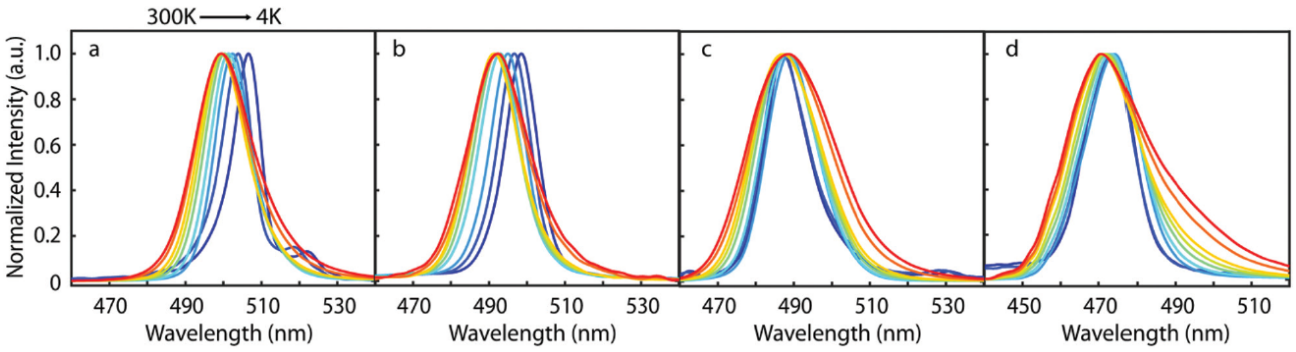

Fig. 3 Normalized steady-state temperature dependent PL spectra of (a) 6.3 nm (b) 5.3 nm (c) 4.7 nm (d) 3.9 nm $CsPbBr_3$ QDs samples at temperatures between 4 and 300 K.

QD films often observe a redshift of the PL attributed to interparticle coupling. The lack of interparticle coupling in this study is likely due to long ligands (oleylammonium bromide) passivating the surface of the QDs, separating them by ~3 nm as can be seen in the TEM images. Fig. 3 shows the normalized temperature-dependent PL spectra of $CsPbBr_3$ QD films collected in the temperature range of 4–300 K for four different sizes. The variation of the peak energy and linewidth with temperature and QD size were analysed from these spectra. For more quantitative analysis of the PL peak energy and linewidth, the experimentally measured PL spectra were converted to the spectral line shape function on an energy axis, $L(E)$, through the Jacobian conversion, where the linewidth is directly proportional to the Franck–Condon factor.[45,46] Both the peak energy and linewidth reported here were extracted from $L(E)$. The details of the conversion and analysis of the PL spectra are provided in the ESI (Fig. S1†).

Fig. 4 shows the temperature-dependent PL peak energy, $E_{peak}(T)$ of $CsPbBr_3$ QDs of four different sizes. All four QDs show generally decreasing $E_{peak}(T)$ with decreases in temperature, which is similar to what has been observed in bulk and large non-confined NCs of $CsPbBr_3$.[40–43,47] On the other hand, the smaller QDs show smaller shift of $E_{peak}(T)$ with temperature and also exhibit a bit more complex behaviour above 200 K, showing a small negative slope of $E_{peak}(T)$ with respect to T although its origin is not clear. Nevertheless, it is notable that the general redshift of $E_{peak}(T)$ with decreasing temperature in $CsPbBr_3$ QDs is opposite to the behaviour of the majority of other semiconductor QDs (*e.g.* such CdSe) that exhibit blueshifts of the exciton absorption and PL peak with decreasing temperature. Furthermore, the slope (dE_{peak}/dT) is significantly smaller than in II–VI QDs of comparable size (−0.3 meV K^{-1} for CdSe QDs and −0.5 meV K^{-1} for CdS QDs).[48,49] Below 200 K, dE_{peak}/dT of $CsPbBr_3$ QDs is 0.05–0.18 meV K^{-1} depending on the size, exhibiting much weaker dependence of E_{peak} on the temperature (0.16, 0.18, 0.05, 0.11 meV for 6.3, 5.3, 4.7, 3.9 nm QDs). The general trend of $E_{peak}(T)$ in LHP NCs can be explained by thermal expansion and exciton–phonon coupling.[50,51] It has been shown that the bandgap decreases with decrease in lattice constant in LHP NCs.[50] The contribution of exciton–phonon coupling is estimated using a two-oscillator model, where acoustic and optical phonons contribute to the temperature dependent bandgap in opposite directions (dE_{peak}/dT >0 for acoustic phonons, <0 for optical phonons), thereby partially cancelling each other. In the framework of the analysis described in ref. 50, non-monotonous variation of $E_{peak}(T)$ in the smaller QDs (d = 5.3, 4.7, 3.9 nm) can be interpreted as resulting from variations in the balance between the two opposing contributions to the bandgap with the QD size.

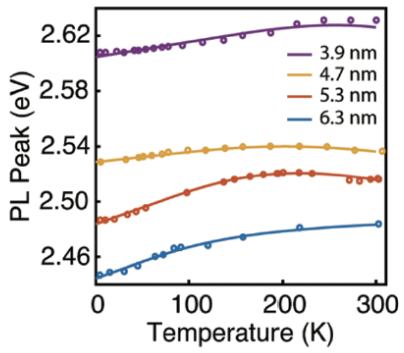

Fig. 4 Temperature-dependent PL peak energy of different sizes of $CsPbBr_3$ QDs samples at temperatures between 4 and 300 K.

Fig. 5 shows the temperature-dependent full-width at half maximum (FWHM), $\Gamma(T)$, determined from the lineshape, $L(E)$, of $CsPbBr_3$ QDs of four different sizes. We employ a linear exciton–phonon coupling model (eqn (1)) commonly used to analyse the temperature dependent $\Gamma(T)$ in order to extract the effective strength of coupling to phonons and the contribution from inhomogeneous broadening.[40,50,52–54]

$$\Gamma(T) = \gamma_{LO}N_{LO} + \gamma_{ac}T + \Gamma_{inh} \quad (1)$$

In this model, $\Gamma(T)$ is expressed as the sum of three terms: temperature-independent inhomogeneous broadening (Γ_{inh}) and temperature-dependent optical ($\gamma_{LO}N_{LO}$) and acoustic ($\gamma_{ac}T$) phonon contributions.γ_{LO} represents coupling strength to longitudinal optical (LO) phonons, which is associated with number of the phonon mode, N_{LO}, described by the Bose–

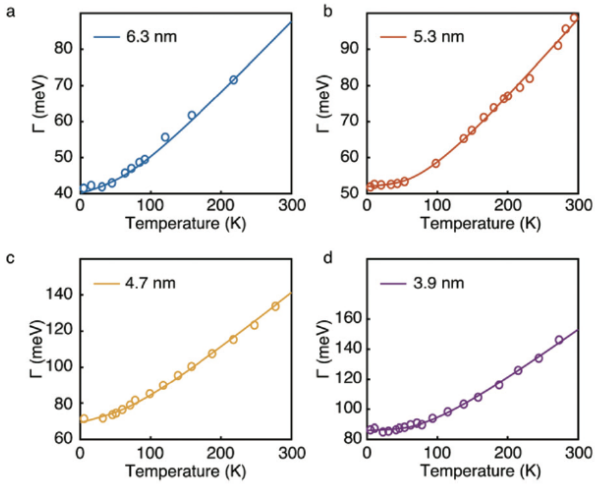

Fig. 5 FWHM of the spectral lineshape as a function of temperature for (a) 6.3 nm (b) 5.3 nm (c) 4.7 nm (d) 3.9 nm QDs. The solid line are fits of eqn (1).

Einstein distribution, $N_{LO} = 1/(exp(E_{LO}/k_bT) - 1)$. Here, E_{LO} is the energy of the LO phonon and k_B is Boltzmann's constant. γ_{ac} represents coupling strength to acoustic phonons, and is mainly related to a deformation potential interaction in materials with cubic symmetry.[54]

Table 1 summarizes the parameters obtained by fitting the experimentally measured $\Gamma(T)$ to eqn (1). Similar to other polar semiconductors, coupling to LO phonons ($\gamma_{LO}N_{LO}$) is the main contribution to the temperature-dependent broadening of the PL linewidth at high temperature ($T > 100$ K). Since the contribution from the acoustic phonon ($\gamma_{ac}T$) accounts for <10% of the total temperature variation of $\Gamma(T)$, we will focus on coupling to LO phonon in our discussion of the size- and temperature-dependent $\Gamma(T)$. The value of E_{LO}obtained from the fit is near 20 meV for QDs of all sizes, and is close to E_{LO} of 19 meV measured from single macroscopic crystals of $CsPbBr_3$.[56] On the other hand, the coupling strength to LO phonons (γ_{LO}) shows a significant size dependence. γ_{LO} increases nearly 3 times (32 to 89 meV) as the size of the QD decreases from d = 6.3 to 3.9 nm. For comparison, γ_{LO} of weakly-confined $CsPbBr_3$ NCs from earlier studies are also added in Table 1, and these values are closer to that of the larger QDs in our study.[40,52] This is an interesting contrast to

Table 1 Extracted linewidth parameters

	Size (nm)	γ_{LO} (meV)	γ_{ac} (μeV K^{-1})	Γ_{inh} (meV)	E_{LO} (meV)
Sample I	6.3	32 ± 13	70 ± 75	40 ± 2.5	20 ± 9
Sample II	5.3	52 ± 13	20 ± 60	52 ± 1.5	21 ± 8
Sample III	4.7	52 ± 18	20 ± 70	69 ± 3	22 ± 11
Sample IV	3.9	89 ± 27	22 ± 50	86 ± 2	23 ± 6
B. Diroll *et al.*[40]	15	45	5	20	19
J. Ramade *et al.*[a 52]	~7	42	8	0.4	16
F. Tang *et al.*[55]	Single crystal	11.61	10	9.02	20.01

[a] Single particle PL.

CdSe QDs that show much smaller and more weakly size-dependent γ_{LO}, therefore exhibiting significantly weaker thermal broadening of PL linewidth and size dependence.[34,37,57] For instance, γ_{LO} of CdSe QDs calculated from the size-dependent Huang-Rhys factor increases very slowly from 10.9 meV to 12.6 meV as the QD size decreases from 5.23 nm to 2.56.[57,58] For a comparable size of QDs (d = ~3.9 nm), $\Gamma(T)$ varies by more than twice as much in $CsPbBr_3$ than in CdSe (46 meV *vs.* 20 meV), within the temperature range of 50–250 K.[59] The stronger coupling of excitons with LO phonons in $CsPbBr_3$ QDs compared to CdSe QDs is not surprising, considering that lead halide perovskite materials are generally known to have larger exciton-phonon coupling.[40,50] The strong exciton-phonon coupling in various inorganic and hybrid lead halide perovskites manifests as facile formation of polarons, which has been shown in both calculations and experiments.[60–62] Strong exciton-phonon coupling was also considered to be responsible for the activation of parity-forbidden exciton transitions in strongly confined $CsPbBr_3$ QDs, whereby polaron formation lifted the optical selection rule.[63]

This strong size-dependence of γ_{LO} in $CsPbBr_3$ QDs is quite intriguing, considering that typical semiconductor QDs such as CdSe QDs exhibit weak size dependence. Earlier studies in various semiconductor QDs showed evidence that increasing the coupling of vibrational modes with surfaces and surface ligands by decreasing size results in the larger effective coupling strength between excitons and vibrational degrees of freedom. For instance, $\Gamma(T)/T$ in 2 nm CdSe QDs increased by 2.2 times by changing the ligand from dodecanethiol to tetradecylphosphonic acid, while such sensitivity to the ligand is absent in much larger QDs.[37] In the case of monolayer WSe_2 and WS_2 QDs, a large increase of $\Gamma(T)$ of the PL at room temperature and Stokes shift was explained by increased coupling of excitons to the chemical bonds at edges with decreasing size.[64,65] Since the model described in eqn (1) does not specifically include the terms representing the coupling of excitons to surface-specific modes, γ_{LO} determined from the fitting represent the combined effect of coupling to both lattice LO phonon mode and local vibrational modes at surface, such as the bond from ligands. This suggests that the strong dependence of γ_{LO} on the size of $CsPbBr_3$ QDs reflect the stronger influence of the surface in coupling with exciton compared to CdSe QDs. At cryogenic temperatures, Γ_{inh} is still relatively large compared to the estimated linewidth broadening based on the QD size distribution determined from the analysis of TEM images (±5% at fwhm) and the experimentally determined size-dependent bandgap.[28] The inhomogeneous linewidth purely from the size distribution is estimated to be <35 meV for the QDs with average size of 4.7 nm. Much larger Γ_{inh} of 69 meV indicates that the inhomogeneous broadening of the PL observed in $CsPbBr_3$ QDs has contribution from not only the size distribution but also from other contributions. While the exact nature of such additional contribution is not clear yet, variations of the surface ligand density or local fluctuation of charges within the film may have contributed to the inhomogeneous broadening.

Conclusion

In summary, the PL spectra of strongly quantum confined $CsPbBr_3$ QDs were measured as a function of size and temperature in order to investigate the factors that determine the spectral evolution with temperature and the degree of quantum confinement. The peak energy of the PL shows much weaker dependence on the temperature for all QD sizes compared to the other well-known semiconductor QDs such as II–VI QDs. On the other hand, the PL linewidth exhibits stronger dependence on both the size of the QD and temperature compared to II–VI QDs, indicating stronger exciton-phonon coupling. γ_{LO} determined from spectral linewidth analysis is several times larger than that of CdSe QDs for comparable sizes, consistent with generally stronger exciton-coupling known for various metal halide perovskite materials in the bulk phase. The size dependence of γ_{LO} is also much stronger than CdSe QDs, indicating the stronger influence of the surface vibrational degrees of freedom for the overall effective exciton-phonon coupling. This detailed information about the dependence of PL spectra on size and temperature will be valuable in applications that employ strongly quantum-confined metal halide perovskite QDs as a source of photons. The effect of varying surface-bound ligands for quantum dots of a given size that can additionally alter the coupling of exciton and vibrational degrees of freedom and change the spectral characteristics will be investigated in future studies.

Conflicts of interest

There are no conflicts to declare.

Acknowledgements

This research was supported by the National Science Foundation (grant no. CHE-1836538, O. H.-C. C.) and Institute for Basic Science (grant no. IBS-R026-D1, D. H. S.). This work was also partially funded by the Gordon and Betty Moore Foundation through Grant GBMF6882. M. S. acknowledges support from the Welch Foundation (A-1886).

References

1 F. Yan and H. V. Demir, *Nanoscale*, 2019, **11**, 11402–11412.
2 M. M. Stylianakis, T. Maksudov, A. Panagiotopoulos, G. Kakavelakis and K. Petridis, *Materials*, 2019, 12.
3 X. Zhang, C. Sun, Y. Zhang, H. Wu, C. Ji, Y. Chuai, P. Wang, S. Wen, C. Zhang and W. W. Yu, *J. Phys. Chem. Lett.*, 2016, 7, 4602–4610.
4 L. Zhang, X. Yang, Q. Jiang, P. Wang, Z. Yin, X. Zhang, H. Tan, Y. M. Yang, M. Wei, B. R. Sutherland, E. H. Sargent and J. You, *Nat. Commun.*, 2017, **8**, 15640.
5 W. Deng, X. Xu, X. Zhang, Y. Zhang, X. Jin, L. Wang, S.-T. Lee and J. Jie, *Adv. Funct. Mater.*, 2016, **26**, 4797–4802.
6 A. Dutta, R. K. Behera, P. Pal, S. Baitalik and N. Pradhan, *Angew. Chem., Int. Ed.*, 2019, **58**, 5552–5556.
7 F. Di Stasio, S. Christodoulou, N. Huo and G. Konstantatos, *Chem. Mater.*, 2017, **29**, 7663–7667.
8 B. A. Koscher, J. K. Swabeck, N. D. Bronstein and A. P. Alivisatos, *J. Am. Chem. Soc.*, 2017, **139**, 6566–6569.
9 B. J. Roman and M. Sheldon, *Chem. Commun.*, 2018, **54**, 6851–6854.
10 F. A. Rodríguez Ortiz, B. J. Roman, J.-R. Wen, N. Mireles Villegas, D. F. Dacres and M. T. Sheldon, *Nanoscale*, 2019, **11**, 18109–18115.
11 G. Nedelcu, L. Protesescu, S. Yakunin, M. I. Bodnarchuk, M. J. Grotevent and M. V. Kovalenko, *Nano Lett.*, 2015, **15**, 5635–5640.
12 D. Parobek, Y. Dong, T. Qiao, D. Rossi and D. H. Son, *J. Am. Chem. Soc.*, 2017, **139**, 4358–4361.
13 A. Sadhanala, S. Ahmad, B. Zhao, N. Giesbrecht, P. M. Pearce, F. Deschler, R. L. Hoye, K. C. Godel, T. Bein, P. Docampo, S. E. Dutton, M. F. De Volder and R. H. Friend, *Nano Lett.*, 2015, **15**, 6095–6101.
14 Y. Miao, Y. Ke, N. Wang, W. Zou, M. Xu, Y. Cao, Y. Sun, R. Yang, Y. Wang, Y. Tong, W. Xu, L. Zhang, R. Li, J. Li, H. He, Y. Jin, F. Gao, W. Huang and J. Wang, *Nat. Commun.*, 2019, 10.
15 T. Chiba, Y. Hayashi, H. Ebe, K. Hoshi, J. Sato, S. Sato, Y.-J. Pu, S. Ohisa and J. Kido, *Nat. Photonics*, 2018, **12**, 681–687.
16 K. Lin, J. Xing, L. N. Quan, F. P. G. de Arquer, X. Gong, J. Lu, L. Xie, W. Zhao, D. Zhang, C. Yan, W. Li, X. Liu, Y. Lu, J. Kirman, E. H. Sargent, Q. Xiong and Z. Wei, *Nature*, 2018, **562**, 245–248.
17 H. Huang, M. I. Bodnarchuk, S. V. Kershaw, M. V. Kovalenko and A. L. Rogach, *ACS Energy Lett.*, 2017, **2**, 2071–2083.
18 Y.-H. Kim, C. Wolf, Y.-T. Kim, H. Cho, W. Kwon, S. Do, A. Sadhanala, C. G. Park, S.-W. Rhee, S. H. Im, R. H. Friend and T.-W. Lee, *ACS Nano*, 2017, **11**, 6586–6593.
19 E. R. Dohner, A. Jaffe, L. R. Bradshaw and H. I. Karunadasa, *J. Am. Chem. Soc.*, 2014, **136**, 13154–13157.
20 J. Mao, H. Lin, F. Ye, M. Qin, J. M. Burkhartsmeyer, H. Zhang, X. Lu, K. S. Wong and W. C. H. Choy, *ACS Nano*, 2018, **12**, 10486–10492.
21 C. Guhrenz, A. Benad, C. Ziegler, D. Haubold, N. Gaponik and A. Eychmüller, *Chem. Mater.*, 2016, **28**, 9033–9040.
22 Y. Su, X. Chen, W. Ji, Q. Zeng, Z. Ren, Z. Su and L. Liu, *ACS Appl. Mater. Interfaces*, 2017, **9**, 33020–33028.
23 H. Zhang, X. Fu, Y. Tang, H. Wang, C. Zhang, W. W. Yu, X. Wang, Y. Zhang and M. Xiao, *Nat. Commun.*, 2019, **10**, 1088.
24 D. J. Slotcavage, H. I. Karunadasa and M. D. McGehee, *ACS Energy Lett.*, 2016, **1**, 1199–1205.
25 P. Vashishtha and J. E. Halpert, *Chem. Mater.*, 2017, **29**, 5965–5973.
26 P. Gratia, G. Grancini, J.-N. Audinot, X. Jeanbourquin, E. Mosconi, I. Zimmermann, D. Dowsett, Y. Lee,

M. Grätzel, F. De Angelis, K. Sivula, T. Wirtz and M. K. Nazeeruddin, *J. Am. Chem. Soc.*, 2016, **138**, 15821–15824.
27 M. C. Brennan, S. Draguta, P. V. Kamat and M. Kuno, *ACS Energy Lett.*, 2018, **3**, 204–213.
28 Y. Dong, T. Qiao, D. Kim, D. Parobek, D. Rossi and D. H. Son, *Nano Lett.*, 2018, **18**, 3716–3722.
29 Y. Dong, T. Qiao, D. Kim, D. Rossi, S. J. Ahn and D. H. Son, *Chem. Mater.*, 2019, **31**, 5655–5662.
30 Q. Li, Y. Yang, W. Que and T. Lian, *Nano Lett.*, 2019, **19**, 5620–5627.
31 M. C. Weidman, A. J. Goodman and W. A. Tisdale, *Chem. Mater.*, 2017, **29**, 5019–5030.
32 Z. Liang, S. Zhao, Z. Xu, B. Qiao, P. Song, D. Gao and X. Xu, *ACS Appl. Mater. Interfaces*, 2016, **8**, 28824–28830.
33 A. Olkhovets, R. C. Hsu, A. Lipovskii and F. W. Wise, *Phys. Rev. Lett.*, 1998, **81**, 3539–3542.
34 D. M. Sagar, R. R. Cooney, S. L. Sewall, E. A. Dias, M. M. Barsan, I. S. Butler and P. Kambhampati, *Phys. Rev. B: Condens. Matter Mater. Phys.*, 2008, 77.
35 S. Nomura and T. Kobayashi, *Phys. Rev. B: Condens. Matter Mater. Phys.*, 1992, **45**, 1305–1316.
36 G. Morello, M. De Giorgi, S. Kudera, L. Manna, R. Cingolani and M. Anni, *J. Phys. Chem. C*, 2007, **111**, 5846–5849.
37 T. G. Mack, L. Jethi and P. Kambhampati, *J. Phys. Chem. C*, 2017, **121**, 28537–28545.
38 N. Yazdani, D. Bozyigit, K. Vuttivorakulchai, M. Luisier, I. Infante and V. Wood, *Nano Lett.*, 2018, **18**, 2233–2242.
39 K. J. Schnitzenbaumer and G. Dukovic, *Nano Lett.*, 2018, **18**, 3667–3674.
40 B. T. Diroll, H. Zhou and R. D. Schaller, *Adv. Funct. Mater.*, 2018, 28.
41 B. Ai, C. Liu, Z. Deng, J. Wang, J. Han and X. Zhao, *Phys. Chem. Chem. Phys.*, 2017, **19**, 17349–17355.
42 J. Li, X. Yuan, P. Jing, J. Li, M. Wei, J. Hua, J. Zhao and L. Tian, *RSC Adv.*, 2016, **6**, 78311–78316.
43 K. Wei, Z. Xu, R. Chen, X. Zheng, X. Cheng and T. Jiang, *Opt. Lett.*, 2016, **41**, 3821–3824.
44 L. Protesescu, S. Yakunin, M. I. Bodnarchuk, F. Krieg, R. Caputo, C. H. Hendon, R. X. Yang, A. Walsh and M. V. Kovalenko, *Nano Lett.*, 2015, **15**, 3692–3696.
45 J. Mooney and P. Kambhampati, *J. Phys. Chem. Lett.*, 2013, **4**, 3316–3318.
46 H.-Y. Chen, S. Maiti, C. A. Nelson, X. Zhu and D. H. Son, *J. Phys. Chem. C*, 2012, **116**, 23838–23843.
47 X. Lao, W. Zhou, Y. Bao, X. Wang, Z. Yang, M. Wang and S. Xu, *Nanoscale*, 2020, **12**, 7315–7320.
48 D. Kim, H. Yokota, K. Shimura and M. Nakayama, *Phys. Chem. Chem. Phys.*, 2013, **15**, 21051–21057.
49 T. Vossmeyer, L. Katsikas, M. Giersig, I. G. Popovic, K. Diesner, A. Chemseddine, A. Eychmueller and H. Weller, *J. Phys. Chem.*, 1994, **98**, 7665–7673.
50 R. Saran, A. Heuer-Jungemann, A. G. Kanaras and R. J. Curry, *Adv. Opt. Mater.*, 2017, **5**, 1700231.
51 C. Yu, Z. Chen, J. J. Wang, W. Pfenninger, N. Vockic, J. T. Kenney and K. Shum, *J. Appl. Phys.*, 2011, 110.
52 J. Ramade, L. M. Andriambariarijaona, V. Steinmetz, N. Goubet, L. Legrand, T. Barisien, F. Bernardot, C. Testelin, E. Lhuillier, A. Bramati and M. Chamarro, *Appl. Phys. Lett.*, 2018, 112.
53 A. D. Wright, C. Verdi, R. L. Milot, G. E. Eperon, M. A. Perez-Osorio, H. J. Snaith, F. Giustino, M. B. Johnston and L. M. Herz, *Nat. Commun.*, 2016, 7.
54 S. Rudin, T. L. Reinecke and B. Segall, *Phys. Rev. B: Condens. Matter Mater. Phys.*, 1990, **42**, 11218–11231.
55 F. Tang, Z. Su, H. Ye, Y. Zhu, J. Dai and S. Xu, *Nanoscale*, 2019, **11**, 20942–20948.
56 C. C. Stoumpos, C. D. Malliakas, J. A. Peters, Z. Liu, M. Sebastian, J. Im, T. C. Chasapis, A. C. Wibowo, D. Y. Chung, A. J. Freeman, B. W. Wessels and M. G. Kanatzidis, *Cryst. Growth Des.*, 2013, **13**, 2722–2727.
57 C. Lin, K. Gong, D. F. Kelley and A. M. Kelley, *J. Phys. Chem. C*, 2015, **119**, 7491–7498.
58 A. M. Kelley, *J. Chem. Phys.*, 2019, **151**, 140901.
59 M. Isarov, N. Grumbach, G. I. Maikov, J. Tilchin, Y. Jang, A. Sashchiuk and E. Lifshitz, *Lith. J. Phys.*, 2016, 55.
60 K. Miyata, D. Meggiolaro, M. T. Trinh, P. P. Joshi, E. Mosconi, S. C. Jones, F. De Angelis and X. Y. Zhu, *Sci. Adv.*, 2017, 3.
61 X. Y. Zhu and V. Podzorov, *J. Phys. Chem. Lett.*, 2015, **6**, 4758–4761.
62 J. M. Frost, *Phys. Rev. B: Condens. Matter Mater. Phys.*, 2017, 96.
63 D. Rossi, H. Wang, Y. Dong, T. Qiao, X. Qian and D. H. Son, *ACS Nano*, 2018, **12**, 12436–12443.
64 H. Jin, M. Ahn, S. Jeong, J. H. Han, D. Yoo, D. H. Son and J. Cheon, *J. Am. Chem. Soc.*, 2016, **138**, 13253–13259.
65 H. Jin, B. Baek, D. Kim, F. Wu, J. D. Batteas, J. Cheon and D. H. Son, *Nano Lett.*, 2017, **17**, 7471–7477.